Advanced synchrotron micro characterization of laser post-processed plasma sprayed LLZO solid-state battery electrolyte

IOP Conf. Series: Materials Science and Engineering **1332** (2025) 012022 doi:10.1088/1757-899X/1332/1/012022

Advanced synchrotron micro characterization of laser post-processed plasma sprayed LLZO solid-state battery electrolyte

Arman Hasani[1]*, Shrikant Joshi[2], Antti Salminen[1], Sneha Goel[3], Antonin Breard[4], Mathias Juan[4], Malgorzata Grazyna Makowska[5], Ermei Mäkilä[6], Chinmayee Nayak[1], Ashish Ganvir[1].

[1]Department of Mechanical and Materials Engineering, Faculty of Technology, University of Turku, Finland.
[2]Department of Engineering Science, University West, Sweden.
[3]Advanced Materials for Nuclear Energy, VTT Technical Research Centre of Finland, Finland.
[4]SeaTech Engineering School, University of Toulon, France.
[5]Paul Scherrer Institute, Laboratory for Synchrotron Radiation and Femtochemistry and Laboratory for Nuclear Materials, Advanced Nuclear Materials Group, Switzerland.
[6]Department of Physics and Astronomy, Faculty of Mathematics and Natural Sciences, University of Turku, Finland.

*E-mail: arman.hasani@utu.fi

Abstract: Garnet-type solid-state electrolytes such as $Li_7La_3Zr_2O_{12}$ (LLZO) offer high ionic conductivity but present challenges in scalable processing due to phase instability and poor interfacial contact. In this study, LLZO thin-film coatings were fabricated via suspension plasma spraying (SPS) and subjected to laser-based thermal post-processing to improve surface and microstructural properties. Synchrotron micro-XRD, along with SEM, EDS, and surface profilometry was employed to analyze the effects of laser post-processing. Results reveal that laser processing reduced surface roughness by up to nearly 40%, eliminated the $La(OH)_3$ phase which is known to increase interfacial resistance, and led to the formation of Li_2ZrO_3 and Li_2CO_3 due to localized remelting. These findings highlight the dual role of laser post-processing in improving both morphological and chemical characteristics of SPS LLZO, offering a promising strategy to enhance solid electrode-solid electrolyte interface quality in solid-state battery architectures.

1. Introduction

Solid-state batteries (SSBs) are widely regarded as a key solution for next-generation electrochemical energy storage, offering improved safety and higher energy density over a broad temperature range. Among these, all-solid-state lithium batteries (ASSLBs) have garnered significant attention, particularly due to their potential for use in electric vehicles and smart grids. Central to ASSLBs are solid-state electrolytes (SSEs), which must exhibit high ionic conductivity, interfacial stability, and chemical durability. However, challenges such as low conductivity, interfacial resistance, mechanical brittleness, and complex, high-cost manufacturing, especially for materials like Lithium Lanthanum Zirconium Oxide (LLZO), which hinders wider societal adoption and commercialization [1–5]. Conventional fabrication methods for LLZO SSEs include

solid-state reaction, sol–gel synthesis, tape casting followed by sintering, and advanced techniques such as spark plasma sintering and hot pressing [6–10]. More recently, plasma spray techniques have emerged as promising alternatives, offering significantly higher deposition rates and potential cost reductions [11,12]. Nevertheless, plasma-sprayed LLZO SSEs often suffer from issues such as phase decomposition, undesired surface roughness, and weak electrode–electrolyte interfaces. Laser-based post-thermal processing has shown promise in improving surface morphology and inducing beneficial phase transformations in plasma-sprayed battery components (e.g., anodes) [13]. Building on this, we hypothesize that similar laser-based post-processing applied to plasma-sprayed LLZO SSEs could enhance surface quality and reduce interfacial resistance by promoting smoother, denser surfaces and improved phase stability.

In this study, we investigate the effects of laser post-processing on suspension plasma-sprayed LLZO SSEs. By varying laser power and scan speed, we evaluate the resulting changes in surface microstructure, roughness, and phase composition using scanning electron microscopy (SEM), energy-dispersive X-ray spectroscopy (EDS), surface profilometry, and synchrotron-based micro-X-ray diffraction (μXRD) [13,14]. Our findings reveal that laser post-processing reduces surface roughness by up to 39.5%, but also induces notable phase decomposition and elemental redistribution at the laser post-processed regions.

2. Experimental Procedure

Lithium Lanthanum Zirconium Oxide ($Li_7La_3Zr_2O_{12}$, LLZO) powder obtained from Toshima Manufacturing Co, Ltd. (Japan) was used as the SSE material for deposition by suspension plasma spraying (SPS). The substrate was commercially pure aluminium ⌀25x2 mm coupon which was grit blasted prior to coating deposition. Table 1 presents the LLZO powder chemical composition determined by EDS and Figure 1 shows the powder morphology observed by SEM. The SPS coating thickness was 35±5 μm.

Table 1. Chemical composition (in Wt.%) of LLZO powder measured by EDS.

Element	Li	La	Zr	O	C	Ca, Si, Cl
Wt.%	nd*	46.0	18.1	25.1	10.7	0.1

(*Li is not detectable with the technique used)

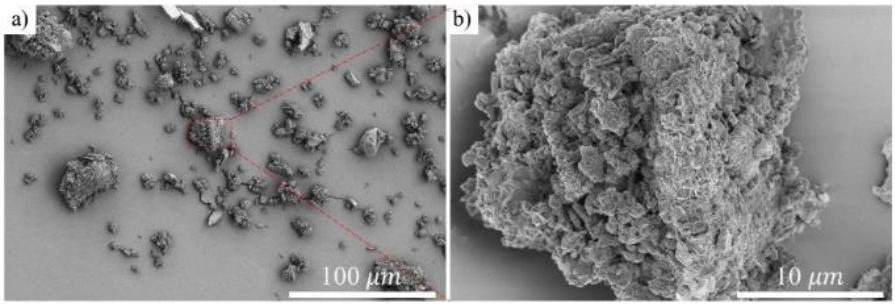

Figure 1. SEM micrographs at (a) low and (b) high magnifications revealing the irregular morphology of LLZO powder.

Thirteen laser-processed lines were created on the top surface of the SPS coating, each corresponding to a distinct set of laser post-processing parameters, as detailed in Table 2. The wavelength and spot size diameter of laser beam were 1070 ±10 nm and 400 μm, respectively. For this study, three representative lines with significantly different energy densities were

selected for detailed analysis. The selection was based on visual inspection and the inclusion of a low input energy condition. The full parameter set is provided in Table 2, with the selected lines L7, R4, and R3 highlighted in blue. These lines are referred to hereafter as Line 1 (L7), Line 2 (R4), and Line 3 (R3), respectively. For further details on experimental procedures about plasma spraying and laser post-processing refer to our previous works [11] [13].

Table 2. Laser post-processing parameters, locations and geometry of the processed lines on the plasma-sprayed coating.

LLZO-SPS laser post-processing conditions											
Lines	Laser power (W)	Laser scanning speed (mm/s)	Energy input (J/mm^2)	Sa (µm)	Delta Sa (%)	Lines	Laser power (W)	Laser scanning speed (mm/s)	Energy input (J/mm^2)	Sa (µm)	ΔSa (%)
L1	56	0.1	713.37	11.60	1.51	R1	111	5	28.28	7.75	34.17
L2	111	0.1	1414.01	8.64	26.63	R2	111	10	14.14	7.45	36.78
L3	111	1	141.40	8.12	30.48	R3(line 3)	222	5	56.56	7.12	39.53
L4	167	1	212.74	7.89	33.04	R4(line 2)	222	10	28.28	7.56	35.77
L5	222	1	282.80	9.11	22.66	R5	333	5	84.84	18.80	-59.60
L6	167	5	42.55	8.72	25.92	R6	333	10	42.42	10.66	9.45
L7 (line 1)	167	10	21.27	7.73	34.33	As-sprayed	-	-	-	11.78	0

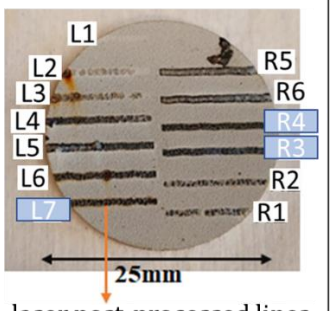

laser post-processed lines

The details of the SEM, EDS, and roughness analysis devices used in this study have been provided in our previous work [13]. The roughness average (Sa) is a dispersion parameter defined as the mean of the absolute values of the surface departure above and below the mean plane within the sampling area [15]. According to Equation 1, ΔSa (%) can take both negative and positive values, indicating roughening and smoothening after laser post-processing, respectively. A higher positive ΔSa (%) value corresponds to a greater degree of surface smoothing.

$$\Delta Sa\ (\%) = \frac{Sa_{As-sprayed} - Sa_{laser\ processed}}{Sa_{As-sprayed}} \times 100 \qquad \text{Equation 1.}$$

To investigate the crystalline phases on the surface of the laser-processed samples, microXRD measurements were carried out at the microXAS beamline of the Swiss Light Source, Switzerland [16]. For a detailed description of the microXRD experiment, including the procedure and equipment, see [14].

3. Results and discussion

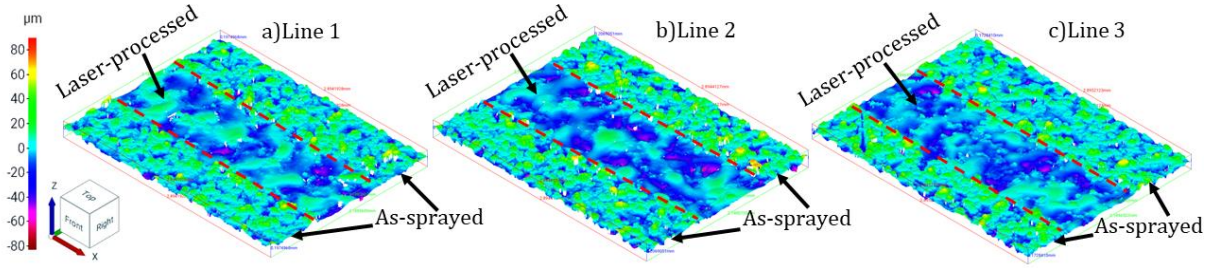

Figure 2. Surface topography of the middle region of laser-processed lines on plasma-sprayed sample, as visualized using optical profilometry: (a) line 1, (b) line 2, (c) line 3.

According to Figure 2 and Table 2, among the 13 laser post-processing conditions, Lines 1, 2, and 3 exhibit both the lowest Sa values and the highest surface roughness reductions (ΔSa) of 34.3%, 35.8%, and 39.5%, respectively. These results reflect the effect of low energy input in achieving significant surface smoothening. Additionally, these lines appeared continuous and uniform, unlike some other low-energy conditions that resulted in discontinuous or irregular tracks (Table 2). However, only among these three selected lines, an increase in energy input leads to a reduction in surface roughness, primarily due to a higher proportion of molten material. This is further supported by the fact that lower scanning speeds allow sufficient time for uniform solidification of the molten regions, resulting in reduced surface roughness. According to Figure 3, laser post-processing induces noticeable changes in the elemental distribution between the laser-processed and as-sprayed regions. In all three selected lines, energy input from the laser leads to localized thermal effects, promoting surface oxidation. As a result, EDS analysis reveals a clear increase in oxygen content in the laser-processed areas compared to the as-sprayed regions. This elevated oxygen presence is accompanied by a relative decrease in the concentrations of Zr and La, likely due to surface oxidation, diffusion, or potential volatilization of these elements during high-temperature exposure. These changes in elemental distribution suggest that laser post-processing not only modifies surface topography but also alters the local chemical environment, which could influence the interfacial properties and electrochemical performance of the SSE.

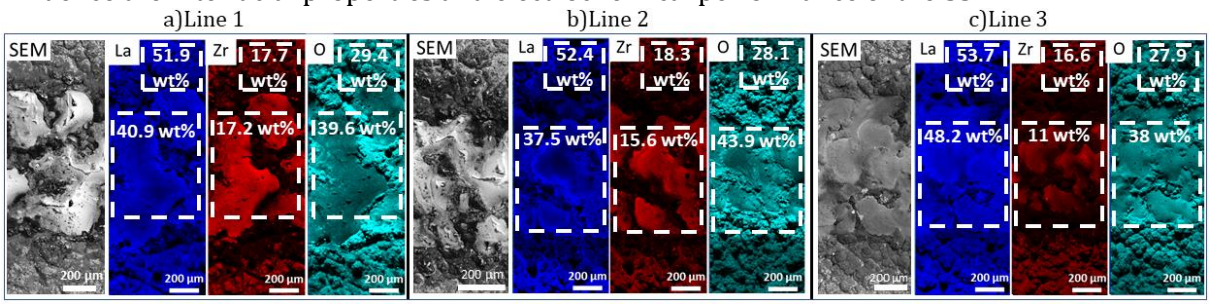

Figure 3. SEM images and corresponding EDS elemental maps for O, Zr, and La, respectively for all the 3 laser-processed lines. Chemical compositions of the laser-processed and neighboring as-sprayed regions are also provided in dashed-line boxes within the figure.

According to Figure 4, the XRD analysis reveals that the as-sprayed SPS LLZO coating retained the primary garnet phase $Li_7La_3Zr_2O_{12}$, indicating partial preservation of the original powder composition during deposition. However, secondary phases such as $La_2Zr_2O_7$ and $La(OH)_3$ also formed due to thermal decomposition during plasma spraying and subsequent exposure to moisture and ambient air. These secondary phases are known to deteriorate the ionic conductivity and chemical stability of the electrolyte, thereby negatively impacting solid-state battery performance.

Laser post-processing introduces further changes in phase composition. The formation of new phases such as Li_2ZrO_3 and Li_2CO_3 in the laser-processed regions suggests that surface remelting and chemical interaction with atmospheric CO_2 and H_2O occurred during high-temperature laser exposure. Li_2CO_3 phase formation can either occur through CO_2 absorption by LiOH phase or the direct reaction of LLZO phase with CO_2 [17]. However, Li_2CO_3 formation leads to high Li/LLZO interfacial resistance, voltage polarization at the Li anode, and the formation of Li dendrites [18].

Furthermore, formation of LiOH and Li_2CO_3 may lead to reduction in ionic conductivity [19]. Notably, the disappearance of $La(OH)_3$ peaks in the laser post-processed samples points to its decomposition or evaporation, consistent with previous reports on its thermal instability [17–20]. This is a particularly beneficial outcome, as $La(OH)_3$ phase is widely recognized in the literature as a detrimental phase that contributes to high interfacial resistance and poor electrochemical performance in garnet-type electrolytes. Therefore, its elimination through laser post-processing can be seen as a positive step toward improving the chemical purity and electrochemical integrity of LLZO-based solid-state electrolytes.

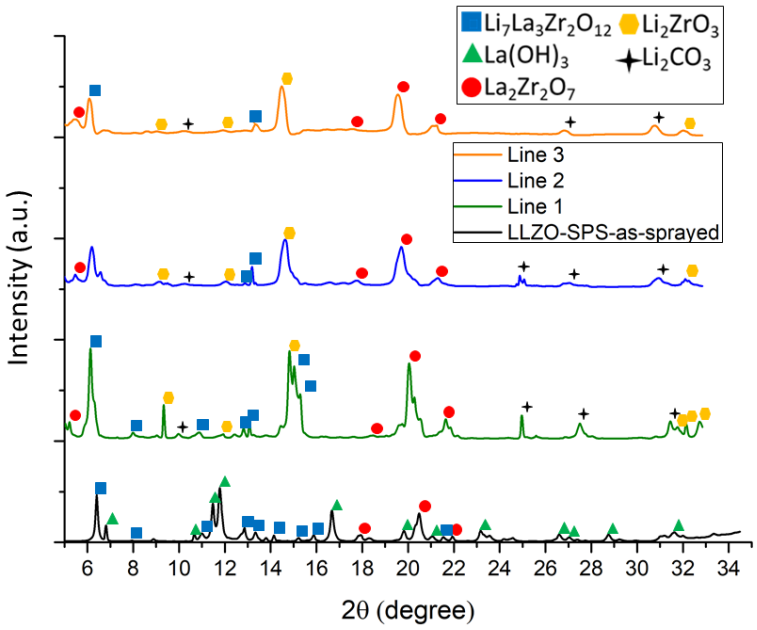

Figure 4. XRD patterns from laser-processed lines and the unprocessed region of SPS as-sprayed LLZO sample, showing phase differences induced by laser processing.

Overall, these findings highlight the dual effect of laser post-processing: it reduces surface roughness and thereby improves electrode–electrolyte contact, and refines the phase composition by eliminating unstable or resistive species such as $La(OH)_3$. However, the simultaneous formation of other decomposition products like Li_2CO_3 warrants careful optimization of laser parameters. Future work should focus on tuning the laser energy input to enhance the beneficial effects of surface and phase modifications while concurrently reducing the generation of detrimental by-products, along with electrochemical testing to directly assess performance improvements.

4. Conclusion

This study demonstrates that laser post-processing is a powerful tool for engineering the surface and phase composition of suspension plasma-sprayed LLZO solid-state electrolytes. By carefully optimizing laser parameters, surface roughness was reduced by up to 40%, which is expected to enhance electrode–electrolyte interfacial contact. Microstructural and elemental analyses revealed that laser treatment introduced localized oxidation and phase transformations, including the removal of detrimental $La(OH)_3$ and the formation of Li_2ZrO_3 and Li_2CO_3. While the elimination of $La(OH)_3$ is beneficial for reducing interfacial resistance, the emergence of Li_2CO_3 necessitates precise control of processing conditions to avoid compromising electrochemical performance. Overall, the findings confirm the dual benefit and complexity of laser post-

processing in tailoring the surface and chemical properties of LLZO coatings, paving the way for improved integration in next-generation all-solid-state batteries. Future studies will focus on electrochemical validation and further process optimization to fully exploit these advantages.

Acknowledgement and Funding

The authors thank Stefan Björklund (University West, Sweden) for plasma spraying support and Aki Piiroinen (University of Turku (UTU)) for laser post-processing assistance. Beamtime at the microXAS beamline was thankfully provided by the Swiss Light Source (SLS), and SEM access was kindly supported by the Materials Research Infrastructure (MARI), UTU. This work was funded by the GREEN-BAT project (2022–2025) under the M-ERA.Net framework, with support from the Research Council of Finland, M-ERA.NET 3 (European Commission), and national/regional funders in Germany and Sweden. Support from European Union Horizon 2020 research and innovation programme under grant agreement No 857470 is also gratefully acknowledged. The Swedish part was additionally supported by the NovelCABs project (Swedish Energy Agency, Dnr 2021-002227) and Vinnova through M-ERA.NET 3. This project also received funding from the EU Horizon 2020 programme (grant agreement No. 958174).

References

[1] Pourzolfaghar H, Wang P, Jiang X, Kositsarakhom S, Jirasupcharoen W, Suwantri C, Jyothi D, Prabhakaran K, Li Y 2024 *Chemical Engineering Journal* **500** 157394, doi: 10.1016/j.cej.2024.157394.
[2] Sung J, Heo J, Kim D, Jo S, Ha Y, Kim D, Ahn S, Park J 2024 *Mater Chem Front* **8** 1861–1887 doi: 10.1039/D3QM01171B.
[3] Shah R, Mittal V, Precilla A M 2024 *J (Basel)* **7** 204–217 doi: 10.3390/j7030012.
[4] Liu Q, Geng Z, Han C, Fu Y, Li S, He Y, Kang F, Li B 2018 *J Power Sources* **389** 120–134 doi: 10.1016/j.jpowsour.2018.04.019.
[5] Xia S, Wu X, Zhang Z, Cui Y, W. Liu 2019 *Chem* **5** 753–785 doi: 10.1016/j.chempr.2018.11.013.
[6] Youssef Dabaki Y, Kassem M, Delaizir G, Sammoury A, Leroy G, Poupin C, Bokova M, Eugene Bychkov 2025 *Ceram Int* **51** 18816-18826 doi: 10.1016/j.ceramint.2025.02.061.
[7] Kern A, McGinn P. J. 2022 *J Eur Ceram Soc* **42** 7501–7507 2022, doi: 10.1016/j.jeurceramsoc.2022.08.054.
[8] Xue J, Zhang K, Chen D, Zeng J, Luo B 2022 *Mater Res Express* **7** 025518 doi: 10.1088/2053-1591/ab7618.
[9] K. Touidjine *et al.*, 2024 *Energy Storage Mater* **71** 103487 2024 doi: 10.1016/j.ensm.2024.103487.
[10] Chen Y.Y, Yan X.X 2025 *Ceram Int* doi: 10.1016/j.ceramint.2025.02.179.
[11] Gopal V, Clovis K, Björklund S, Balapure A, Goel S, Hall A, Younesi R, Joshi S 2025 *Surf Coat Technol* **502** 131945 doi: 10.1016/j.surfcoat.2025.131945.
[12] Koresh I, Klein B. A, Tang Z, Michaelis V. K, Troczynski T 2022 *Solid State Ion* **380** 115938 doi: 10.1016/j.ssi.2022.115938.
[13] Hasani A, Luya M, Kamboj N, Nayak C, Joshi S, Salminen A, Goel S, Ganvir A 2024 *Coatings* **14** 224 doi: 10.3390/coatings14020224.
[14] Hasani A, Joshi S, Salminen A, Goel S, Reuteler J, Makowska M.G, Ganvir A 2025 *Journal of Thermal Spray Technology* doi: 10.1007/s11666-025-02003-6.
[15] Semnani D, 2017 *Electrospun Nanofibers* 151–180 doi: 10.1016/B978-0-08-100907-9.00007-6.
[16] Borca C.N, Grolimund D, Willimann M, Meyer B, Jefimovs K, Vila-Comamala J, David C 2009 *J Phys Conf Ser* **186** 012003 doi: 10.1088/1742-6596/186/1/012003.
[17] A. Sharafi *et al.* 2017 *J Mater Chem A Mater* **5** 13475–13487 doi: 10.1039/C7TA03162A.
[18] H. Zhang *et al.*, 2023 *ACS Appl Energy Mater* **6** 6972–6980 doi: 10.1021/acsaem.3c00459.
[19] Ghorbanzade P, Pesce A, Gómez K, Accardo G, Devaraj S, López-Aranguren P, López del Amo J.M 2023 *J Mater Chem A Mater* **11** 11675–11683 doi: 10.1039/D3TA01145C.
[20] Ghorbanzade P, López-Aranguren P, López del Amo J. M 2024 *ChemElectroChem* **11** doi: 10.1002/celc.202400136.